Journal of Applied Polymer Science

# Morphology, structure, and photovoltaic properties of poly(3-hexylthiophene) and [6,6]-phenyl-C61-butyric acid methyl ester-based ternary blends doping with polystyrene of different tacticities

**Jiangman Shi,[1] Weihua Zhou,[1,2] Lin Zhang,[2] Kunxing Hu,[2] Yuanpeng Xie[2]**

[1]Institute of Polymers, Nanchang University, Nanchang 330031, China

[2]State Key Laboratory of Luminescent Materials and Devices, South China University of Technology, Guangzhou 510640, China

Correspondence to: W. Zhou (E-mail: zhouweihua@ncu.edu.cn)

**ABSTRACT:** The influence of the polystyrene of different tacticities on the morphology, phase structure, and photovoltaic properties of poly(3-hexylthiophene) (P3HT) and [6,6]-phenyl-C61-butyric acid methyl ester (PCBM) blend has been extensively investigated. The atactic polystyrene (aPS) immiscible with P3HT tended to form the phase-separated and columnar structure at low aPS weight ratio. Besides, the aPS could migrate to the surface of the films with PCBM phase distributing in the interfaces between P3HT and aPS domains at high aPS weight ratio of 75 wt %. The syndiotactic polystyrene (sPS) immiscible with P3HT could induce the crystallization of P3HT at low weight ratio of 3 wt %. The device based on aPS/P3HT/PCBM ternary blend showed of power conversion efficiency (PCE) of 1.2% even at aPS weight ratio of 50 wt %. However, the device based on sPS/P3HT/PCBM exhibited a sharp decrease in PCE value from 2.3% to 0.6% at sPS weight ratio of 3 wt %, due to the change in film morphology. The performance of the solar cell is believed to be determined by the morphology and phase structure of the ternary blends as revealed by the atomic force microscopy and UV-vis spectra analysis. © 2015 Wiley Periodicals, Inc. J. Appl. Polym. Sci. **2015**, *132*, 41823.

**KEYWORDS:** blends; crystallization; morphology; optical and photovoltaic applications; polystyrene

Received 14 July 2014; accepted 28 November 2014

**DOI: 10.1002/app.41823**

## INTRODUCTION

With the rapid development of organic electronics, polymer photoelectric devices based on organic semiconductor systems have been extensively studied over the last two decades.[1–4] In particular, bulk heterojunction (BHJ) polymer solar cells have gained much attention because of their potential advantages, including low-cost, light weight, flexibility, the possibility of creating large-area roll-to-roll devices and for commercial applications.[5,6] One of the most widely studied systems of active layer is a blend of regioregular poly(3-hexylthiophene) (P3HT) and [6,6]-phenyl-C61-butyric acid methyl ester (PCBM) in organic solar cells. The crystallization and phase separation of this binary blend and the consequent effects on photovoltaic performance has been investigated extensively.[7–9] Although successive improvement in efficiency, polymer bulk heterojunction solar cells based on P3HT/PCBM blend still suffer from two major shortcomings: a poorly controlled donor and acceptor domain size distribution and mechanical and environmental instability under flexing or heating. To improve the photoelectric performance, one of the commonly used techniques in modifying the active layers is ternary blend, by the incorporation of various compounds that are designed to remain in the active layer as a third component added to the blend.[10–12] The presence of such additives can introduce additional functionalities and productively alter the morphology of the active layer.

As a typically third component in the P3HT/PCBM system, the organic dye molecules were reported to broaden the absorption range of sunlight,[13,14] the nanoparticles[15,16] and carbon nanotubes[17,18] were demonstrated to improve the crystallization of P3HT, leading to enhanced exciton dissociation and carrier mobility as well as the short circuit current density ($J_{sc}$) value. However, in the ternary polymer solar cells (PSCs), the insulating polymers were less adopted as a third component. The addition of an insulating polymer dilutes the concentration of donor and acceptor components to reduce the absorbance of an active layer and may disrupt the continuous pathways of donor and acceptor phase, thereby stopping the transport of charges to the electrodes of a solar cell. Recently, addition of an inert polymer has demonstrated to facilitate the fabrication of low-percolation threshold field-effect transistor (FET) devices of

organic semiconducting small molecules, oligomers, and polymers.[19–25] It is revealed that the addition of an inert component appears to have a less detrimental effect on the electronic properties of conjugated polymers[25] than on those of small molecules.[21] Several studies indicated that the semiconducting polymer was able to form more continuous pathways, leading to enhanced output on-current and charge mobility of transistors upon the introduction of an insulating polymer.[26–28] Moreover, the leakage current of a transistor could be reduced,[26–28] and the stability under operation whether for a long term or in the air could be improved by incorporating an insulating polymer in the active layer.[24,29,30]

Incorporating insulating polymers into intrinsic organic semiconductor does reduce cost, increase flexibility as well as improve environmental stability of semiconductor-based electronics. For example, about 50 wt % of the insulating semicrystalline high-density polyethylene and isotactic polystyrene (iPS) have been respectively incorporated into P3HT/PCBM system without seriously reducing performance of devices, facilitating the improvement of processing and mechanical properties.[31] Moreover, the P3HT chain conformations became more homogeneous and suppressed the formation of vacancies and leakage pathways after the incorporation of poly(methyl methacrylate) (PMMA).[32] Other ternary blend films of PS/P3HT/PCBM in a 1 : 1 : 1 weight ratio has been reported that a columnar structure was achieved by phase separation between polystyrene and P3HT with the PCBM mostly aggregated at the interface of two phases. The structure provides the large interfacial area between electron donor and acceptor, which enhances the exciton dissociation efficiency and carrier transportation, leading to the higher efficiency.[33] By taking advantage of the spontaneous phase separation between P3HT and PS, a vertically nanoporous structures of P3HT over large areas could be obtained. And the bilayer BHJ device of the highest power conversion efficiency (PCE) value of 3.25% could be achieved after removal of PS phase and deposition of PCBM.[34]

Atactic polystyrene (aPS), an amorphous polymer, was widely used in binary or ternary blend system.[35,36] The phase separation and dewetting process in thin blend films can construct a great variety of morphologies, such as the vertical phase separation to a layered structure by changing the aPS concentration, which achieve different surface and interface morphologies. The blends based on amorphous polymers involve only phase separation and dewetting during the film fabrication process. When a crystalline polymer is introduced into the polymer blends, the effect of crystallization on the morphology is of interest because the interplay of crystallization, phase separation, and dewetting processes during spin coating may lead to different morphology compared to that of glassy polymer blends. The phase-separation morphology and the performance of P3HT/PCBM-based ternary blend films have been well studied. However, most of the current studies focused on the atactic polystyrene, little attention have paid to the polystyrene with different tacticities, such as syndiotactic polystyrene (sPS). As compared with its isomeric counterpart aPS and iPS, sPS is a fast crystallizing polymer possessing a high melting temperature of about 270°C, which could be used as the engineering plastic.[37] The effect of the polystyrene with different tacticities on the crystallization, phase separation and dewetting behavior of P3HT/PCBM has not been explored. In addition, the relationship between the morphology of the active layer and the photovoltaic performance in the ternary blend system is not well understood.

In this article, the aPS and sPS were incorporated into the P3HT/PCBM system via the solution blending method. The incorporation of polystyrene into P3HT/PCBM system may increase the mechanical strength, stability on exposure to air and reduce the cost.[31,38,39] The influence of the weight ratios, thermal annealing treatment and tacticities of polystyrene on the morphology and phase separation in active layer, in addition to the interactions between the components was extensively analyzed. The aPS/P3HT/PCBM system showed of relatively good photovoltaic performance even at aPS doping ratio of 50 wt %. However, the sPS deteriorated the PCE value of P3HT/PCBM even at doping ratios below 10 wt %. This study illustrate that the tacticity of polystyrene played a vital role on the morphology and performance of the ternary blend PSCs.

## EXPERIMENTAL

### Materials and Equipments

Regioregular P3HT (>90.0%; HT, head to tail) and PCBM used in this study were purchased from Nano-C and Rieke Metals, respectively. The aPS was PG-79 from Zhenjiang CHIMEI Chemical of China, and the weight-average molecular weight ($M_w$) was 54 000 g/mol. The sPS was Questra F2250 from Dow Chemical, and the $M_w$ was $2.3 \times 10^5$ g/mol. Indium tin oxide (ITO) glass was purchased from Delta Technologies Limited, whereas PEDOT : PSS (Baytron PAl4083) was obtained from Bayer Dicholorobenzene (DCB) and 1,2,4-trichlorobenzene (TCB) were purchased from Aldrich. All the reagents were used directly as received without further purification.

The miscibility and interactions between P3HT, PCBM, and aPS (or sPS) were characterized by the differential scanning calorimetry (DSC) analysis. All the pure and blending samples were prepared by the solution blending method in chloroform. After evaporation of the solvents and drying at room temperature under vacuum for 24 h, the corresponding specimens of about 3 mg were heated to 300°C at a rate of 10°C/min under nitrogen protection, followed by cooling to room temperature at a rate of 10°C/min. Consequently, the specimens were heated to 300°C at 10°C/min to afford the corresponding heating and cooling curves. The morphology of the films was observed by the polarized optical microscopy (POM) (NIKON E600 POL) equipped with a camera. The atomic force microscopy (AFM) images were measured on a Nanoscope III A (Digital Instruments) scanning probe microscope using the tapping mode. The morphology of the films was conducted by employing transmission electron microscopy (JEM-2010 HR) with an accelerating voltage of 200 kV. The out-of-plane grazing-incidence X-ray diffraction (GIXRD) profiles were obtained by using a Bruker D8 Discover reflector with an X-ray generation power of 40 kV tube voltage and 40 mA tube current. The measurements were obtained in a scanning interval of $2\theta$ between 2° and 30°. The UV-visible absorption spectra of aPS/P3HT/PCBM and sPS/P3HT/PCBM films were obtained using a

Perkin–Elmer Lambda 750 UV/VIS spectrometer. Photocurrent/voltage (*J*/*V*) curves were recorded using a Keithley 2400 Source Meter under 100 mW/cm$^2$ simulated AM 1.5 G irradiation (Abet Solar Simulator Sun2000). All the measurements were performed under ambient atmosphere at room temperature.

### Methods

**Preparation of Films.** The aPS, P3HT, and PCBM with weight ratios of 0.03 : 1 : 1, 0.05 : 1 : 1, 0.10 : 1 : 1, 1 : 3 : 3, 1 : 1 : 1 and 3 : 1 : 1 were dissolved in o-dichlorobenzene, followed by stirring at 50°C for 2 h to ensure absolute dissolution. The sPS, P3HT, and PCBM with weight ratios of 0.03 : 1 : 1, 0.05 : 1 : 1, 0.10 : 1 : 1, 1 : 3 : 3, 1 : 1 : 1, and 3 : 1 : 1 were dissolved in 1,2,4-trichlorobenzene, followed by stirring at 120°C for 8 h to ensure absolute dissolution. Then, the solution was spin-coated onto an ITO glass at a spin rate of 800 rpm for 25 s and the specimens were dried in a vacuum oven for 2 h. Then, the specimens were further annealed at 150°C for 10 or 120 min under nitrogen protection, respectively.

**Device Fabrication.** The polymer solar cell devices were fabricated on ITO glass as follows. ITO glasses were cleaned in acetone, detergent, de-ionized water, and isopropyl alcohol sequentially, and then cleaned with a UV $O_3$ cleaner (Nippon Laser & Electronics NL-UV253S) for 30 min. PEDOT : PSS was immediately spin-coated onto the cleaned substrates at a spin rate of 3000 rpm. Then, the PEDOT : PSS film was transferred to a glove box filled with $N_2$ gas after heating on a hot plate at 140°C for 20 min. Then, 60 $\mu$L of the solutions of aPS/P3HT/PCBM in DCB were spin-casted onto the top of the PEDOT : PSS layer at a spin rate of 800 rpm for 25 s. The concentration of P3HT was maintained at 10 mg/mL. After drying in the glove box, the specimens were annealed at 150°C for 10 min to give an active layer with a thickness of about 120 nm. Similarly, 60 $\mu$L of the solutions of sPS/P3HT/PCBM in TCB were spin-casted onto the top of the PEDOT : PSS layer at a spin rate of 800 rpm for 25 s, to afford an active layer with the thickness of about 120 nm after thermal annealing at 150°C for 10 min. A cathode consisting of a LiF (1 nm) layer and a subsequent Al (100 nm) layer was deposited by thermal evaporation under a vacuum of $10^{-7}$ Torr. Devices with the configuration of ITO/PEDOT : PSS/aPS(sPS) : P3HT : PCBM/LiF/Al were encapsulated with a glass cap to protect them from air. The active area of all of the devices was defined as 4 mm$^2$ by a shadow mask.

## RESULTS AND DISCUSSION

### Morphology and Phase Structure of aPS/P3HT/PCBM Ternary Blending Films

The interactions between the aPS, P3HT, and PCBM are actually not well understood. As shown in Figure 1(a), aPS exhibits a glass transition on the DSC heating curve, and the P3HT shows of a melting peak at around 218.7°C. Three melting peaks could be discerned for pristine PCBM. In the aPS/P3HT blend, one relatively minor melting peak at 221.6°C is noticed, showing that the crystallization of P3HT from the solution is not seriously disturbed by the aPS. Furthermore, in the aPS/PCBM blend, one melting peak at 281.3°C attributing to PCBM was observed. It is noted that one endothermic peak at 117.8°C is present on the DSC heating curves, which could be

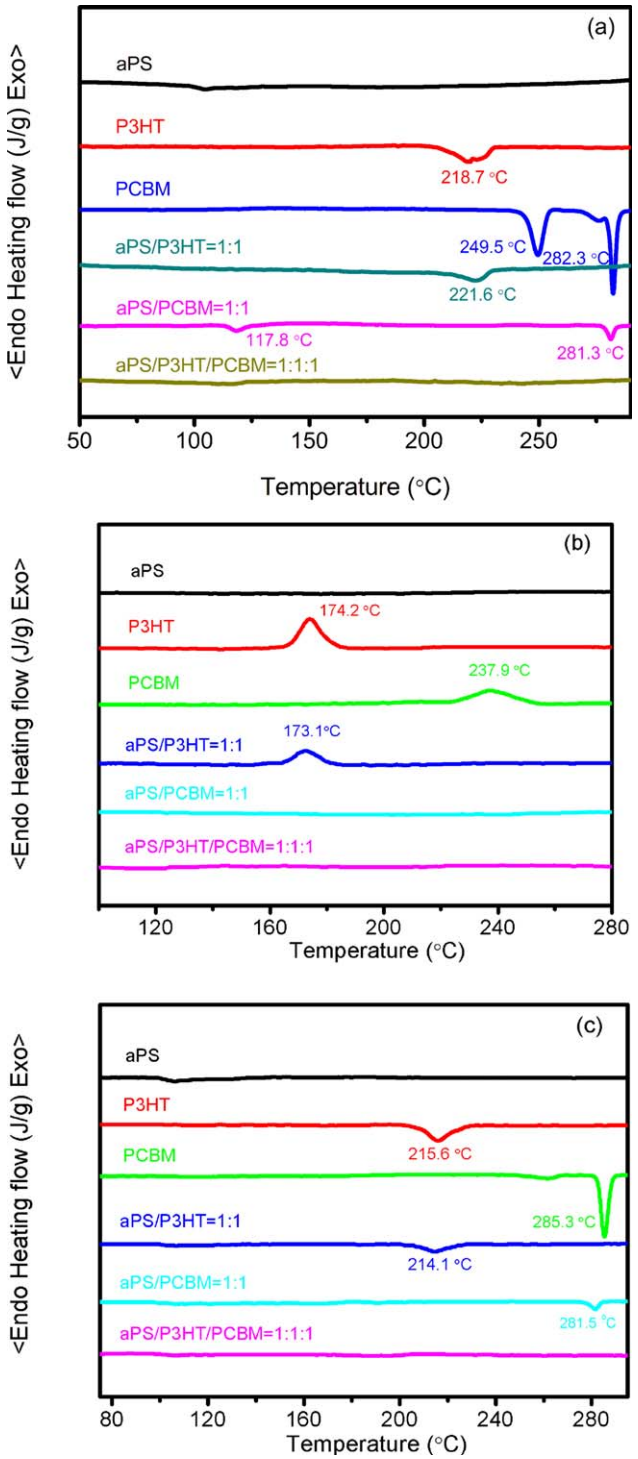


**Figure 1.** DSC (a) heating, (b) cooling, and (c) second heating curves for aPS, P3HT, PCBM. and their blends. [Color figure can be viewed in the online issue, which is available at wileyonlinelibrary.com.]

related to the complexes composing of aPS and PCBM because of the strong interactions between the phenyl groups of aPS and PCBM. In the aPS/P3HT/PCBM ternary blend, no significant thermal transition signals could be observed, illustrating that the crystallization of P3HT and PCBM was restricted by each other. Additionally, the incorporation of aPS significantly

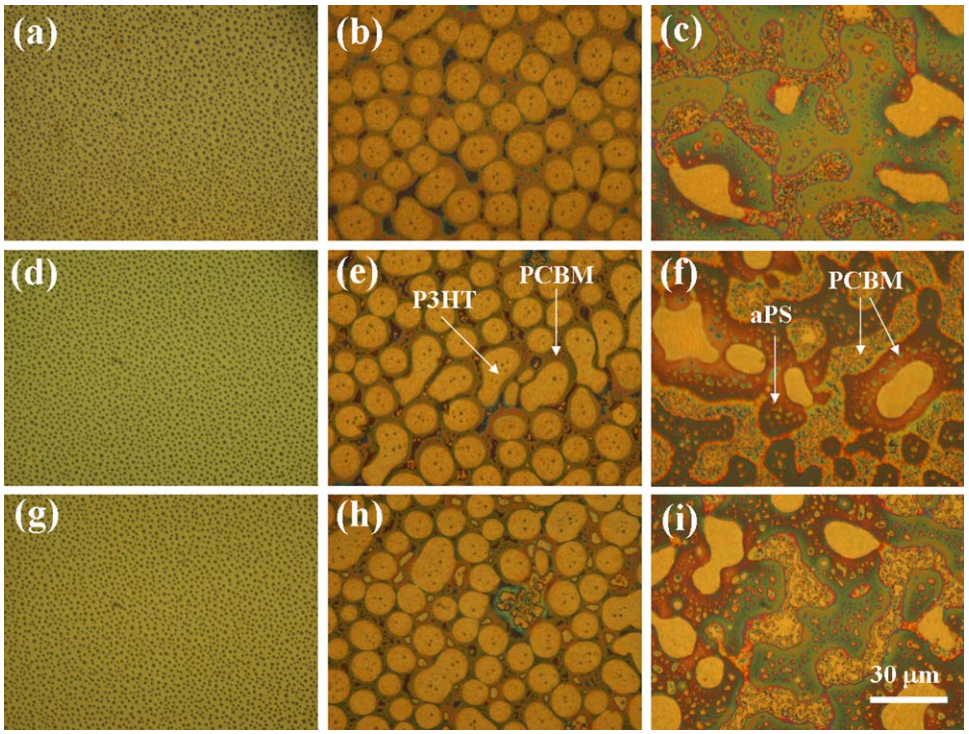


**Figure 2.** POM images of aPS/P3HT/PCBM films at different weight ratios after various thermal treatments. The as-cast specimens of (a–c) 1 : 3 : 3, 1 : 1 : 1, 3 : 1 : 1, the specimens of (d–f) 1 : 3 : 3, 1 : 1 : 1, 3 : 1 : 1 after annealing at 150°C for 10 min, and the specimens of (g–i) 1 : 3 : 3, 1 : 1 : 1, 3 : 1 : 1 after annealing at 150°C for 60 min, respectively. [Color figure can be viewed in the online issue, which is available at wileyonlinelibrary.com.]

affected the crystallization behavior of P3HT and PCBM as cooling from the melting state [Figure 1(b)]. For example, the crystallization peak of P3HT shifts to lower temperature, indicating that the presence of aPS dilutes the concentration of P3HT. Moreover, no exothermic peak contributing to the crystallization of PCBM could be observed for the aPS/PCBM blend. The presence of aPS is believed to restrict the crystallization of PCBM from the melting state because of the strong

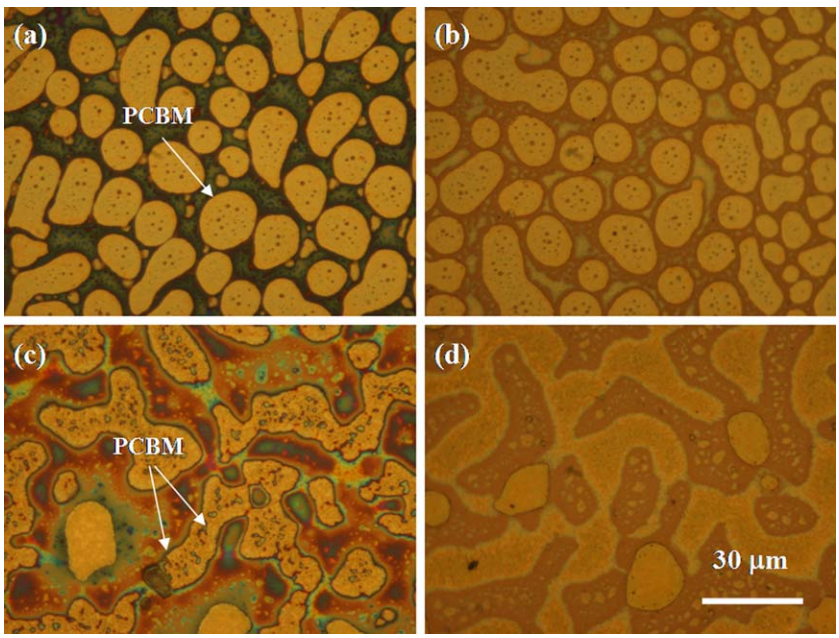


**Figure 3.** POM images of aPS/P3HT/PCBM blending films after soaking into acetone to remove the aPS phase (a, c), and soaking into cyclohexanone to remove the PCBM phase (b, d) successively, the specimens of (a, b) 1 : 1 : 1 and (c, d) 3 : 1 : 1 after annealing at 150°C for 10 min, respectively. [Color figure can be viewed in the online issue, which is available at wileyonlinelibrary.com.]

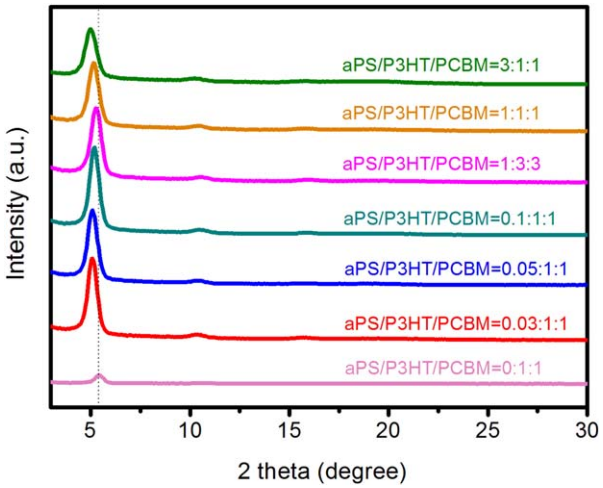


**Figure 4.** Out-of-plane GIXRD profiles of the aPS/P3HT/PCBM blending thin films after thermal annealing at 150°C for 10 min. [Color figure can be viewed in the online issue, which is available at wileyonlinelibrary.com.]

interactions of the phenyl groups in aPS molecular chains with PCBM molecules. Additionally, the aPS/P3HT/PCBM ternary blend showed of no significant crystallization peak as cooling from the melting state. It is concluded that the existence of aPS shows of no significant effect on the crystallization of P3HT but seriously restricts the crystallization of PCBM. Figure 1(c) shows of the second heating curve of the specimens after removal of thermal history. It is noted that the melting temperature of P3HT slightly decreases for both pristine P3HT and its blend with aPS. The melting temperature of PCBM remains almost constant for the aPS/PCBM blend, and the endothermic peak at 117.8°C disappears because of the removal of thermal history.

Based on the DSC analysis, the aPS is supposed to have stronger interactions with PCBM than P3HT. Thus, the morphology and phase structure of the ternary blends at different weight ratios of aPS was investigated by the POM. As shown in Figure 2, the aPS weight ratio and the thermal annealing treatment significantly influence the morphology of the ternary films. It is observed that the aPS and P3HT are immiscible, and the dark regions contributing to aPS phase distributes homogeneously in the P3HT matrix for the aPS/P3HT/PCBM (1 : 3 : 3) specimen [Figure 2(a)]. In addition, the spherical domains composing of P3HT are well distributed in the continuous phase of aPS for the aPS/P3HT/PCBM (1 : 1 : 1) specimen [Figure 2(b)], illustrating of the formation of columnar structure according to Rafailovich *et al.*[33] It is noted that the boundaries between the separated and continuous phase are not obvious. Further increase of the aPS doping ratio leads to the irregular distribution of P3HT phase in the aPS matrix [Figure 2(c)]. After thermal annealing treatment at 150°C for 10 and 60 min, the morphology for the aPS/P3HT/PCBM (1 : 3 : 3) specimen showed of no significant change as compared with the as-cast sample. An obvious rim was observed between the P3HT and aPS phase for the aPS/P3HT/PCBM (1 : 1 : 1) specimen, which should be contributed to the PCBM phase.[33] Regardless of the polymer phase where the PCBM is placed initially, a layer will be formed at the phase interface to reduce the overall energy of the system. Thus, there is a slight repulsion between the nanoparticles and the aPS phase, resulting in almost no nanoparticles diffusing to that phase when they are started out in the P3HT phase. For the aPS/P3HT/PCBM (3 : 1 : 1) specimen, the P3HT phase seems to be more anisotropic, because of the formation of crystalline phase [Figure 2(f,i)]. During the thermal annealing treatment, the PCBM molecules tend to migrate to the interfaces between P3HT and aPS and crystallize to form PCBM crystals. Moreover, the existence of large amount of aPS may lead to the migration of aPS phase onto upper layer and P3HT phase remaining on the bottom layer.[36] Thus, the anisotropic phase in the POM image should be because of the enrichment of PCBM phase between the interfaces of P3HT and aPS domains. The annealing time seems to have no significant influence on the morphology evolution of the ternary blend films.

**Table I.** Photovoltaic Properties of BHJ PSCs Based on aPS/P3HT/PCBM and sPS/P3HT/PCBM Blend Films at Different PS Weight Ratios after Annealing at 150°C for 10 min

| | PS/P3HT/PCBM | $J_{sc}$ (mA/cm$^2$) | $V_{oc}$ (V) | FF (%) | PCE (%) | CCL[a] (nm) |
|---|---|---|---|---|---|---|
| aPS | 0 : 1 : 1 | 6.59 ± 0.20 | 0.606 ± 0.010 | 56.6 ± 2 | 2.3 ± 0.1 | 15.33 |
| | 0.03 : 1 : 1 | 6.22 ± 0.15 | 0.614 ± 0.010 | 57.3 ± 2 | 2.2 ± 0.1 | 14.68 |
| | 0.05 : 1 : 1 | 5.94 ± 0.15 | 0.629 ± 0.015 | 57.7 ± 2 | 2.2 ± 0.1 | 14.42 |
| | 0.10 : 1 : 1 | 5.52 ± 0.10 | 0.631 ± 0.015 | 58.9 ± 2 | 2.1 ± 0.2 | 14.26 |
| | 1 : 3 : 3 | 4.29 ± 0.10 | 0.617 ± 0.010 | 47.4 ± 2 | 1.3 ± 0.2 | 13.41 |
| | 1 : 1 : 1 | 3.77 ± 0.15 | 0.623 ± 0.015 | 49.0 ± 2 | 1.2 ± 0.2 | 12.95 |
| | 3 : 1 : 1 | 1.16 ± 0.10 | 0.633 ± 0.010 | 48.6 ± 2 | 0.4 ± 0.1 | 11.99 |
| sPS | 0.03 : 1 : 1 | 3.33 ± 0.20 | 0.418 ± 0.010 | 40.5 ± 2 | 0.6 ± 0.1 | 12.44 |
| | 0.05 : 1 : 1 | 2.94 ± 0.20 | 0.379 ± 0.010 | 40.8 ± 2 | 0.5 ± 0.1 | 11.71 |
| | 0.10 : 1 : 1 | 2.24 ± 0.15 | 0.346 ± 0.010 | 41.0 ± 2 | 0.3 ± 0.1 | 10.77 |
| | 1 : 3 : 3 | 0.53 ± 0.15 | 0.201 ± 0.010 | 32.5 ± 2 | 0 | 9.74 |
| | 1 : 1 : 1 | 0.02 ± 0.10 | 0.345 ± 0.010 | 12.7 ± 2 | 0 | 10.13 |
| | 3 : 1 : 1 | 0.01 ± 0.15 | 0.480 ± 0.010 | 13.2 ± 2 | 0 | 9.50 |

[a] The crystalline correlation length (CCL) of P3HT was calculated from Scherrer's equation by fitting the diffraction peaks.

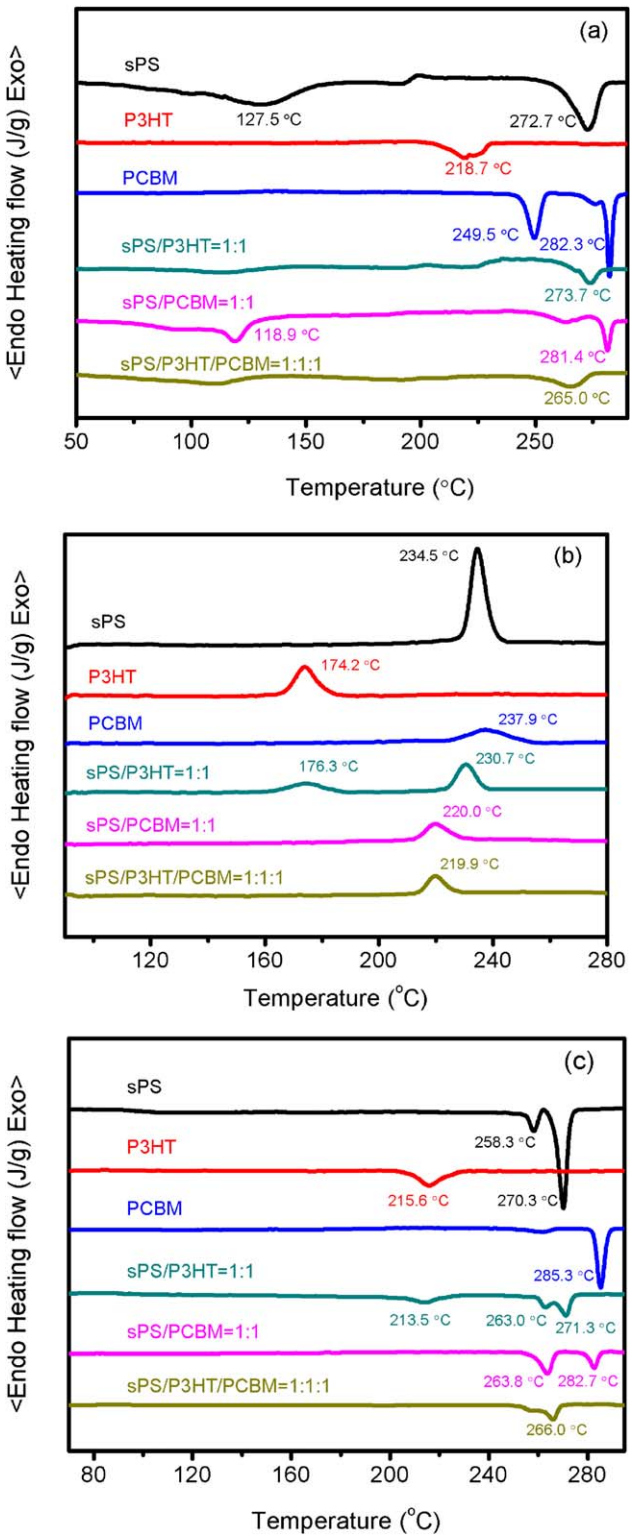


**Figure 5.** DSC (a) heating, (b) cooling, and (c) second heating curves for sPS, P3HT, PCBM, and their blends. [Color figure can be viewed in the online issue, which is available at wileyonlinelibrary.com.]

In order to further confirm the phase structure in the ternary blend films, the specimens were soaked into different solvents to remove the aPS phase and PCBM phase. As acetone is a solvent for aPS but not for P3HT, it can be used to selectively remove the aPS domains from the phase-separated films. By soaking into the acetone, the aPS phase was removed, showing of dark areas in the POM image [Figure 3(a)]. Moreover, the PCBM phase between the interface of P3HT and aPS phases becomes more obvious after removal of aPS, indicating of aPS layer on the surface of films [Figure 3(c)]. Then, after soaking into cyclohexanone solvent, the PCBM phase was removed. In Figure 3(b), the rim phase around the spherical P3HT phase could not be observed. In Figure 3(d), the rim phase and the crystalline phase all disappeared, confirming of the successful removal of PCBM phase. Based on the above results, it is suggested that the aPS and P3HT tend to form the phase-separated and columnar structure at low aPS weight ratio. Besides, the aPS could migrate to the surfaces of the films with PCBM phase distributing in the interfaces between P3HT and aPS domains at high aPS weight ratio.

The GIXRD was further used to characterize the crystalline structure of the ternary blend films as shown in Figure 4. The pristine P3HT/PCBM film exhibits a minor diffraction peak at 5.4°, with the lamellar spacing calculating to be 1.63 nm. Upon incorporation of aPS, the diffraction peak ascribing to P3HT shifted to lower angles and the peak intensity became stronger in contrast to P3HT/PCBM specimen. The lamellar spacing of P3HT in aPS/P3HT/PCBM (0.03 : 1 : 1) and aPS/P3HT/PCBM (3 : 1 : 1) is calculated to be 1.73 and 1.76 nm, respectively. It is revealed that the molecular chain packing of P3HT was influenced by the incorporation of aPS, and the aPS at low weight ratio is supposed to induce the crystallization of P3HT. To further investigate the effect of aPS on the crystal size of P3HT, the crystalline correlation length (CCL) of P3HT was calculated from Scherrer's equation by fitting the diffraction peaks:

$$\mathrm{CCL} = \frac{2\pi}{\mathrm{FWHM}} \quad (1)$$

where FWHM is the full-width-at-half-maximum of the fitted Pseudo-Voigt function. The CCL is a measure of crystallite size and/or perfection.[40] The calculated parameters are shown

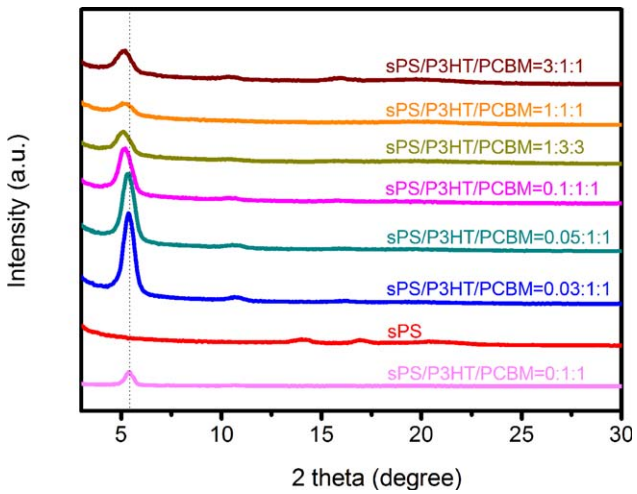


**Figure 6.** Out-of-plane GIXRD profiles of the sPS/P3HT/PCBM blending thin films after thermal annealing at 150°C for 10 min. [Color figure can be viewed in the online issue, which is available at wileyonlinelibrary.com.]

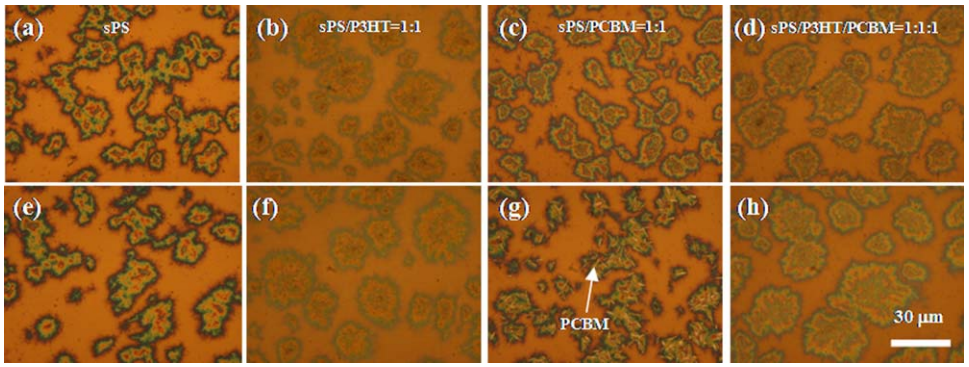


**Figure 7.** POM images of the as-cast (a) sPS, (b) sPS : P3HT=1 : 1, (c) sPS : PCBM=1 : 1 and (d) sPS : P3HT : PCBM=1 : 1 : 1 films and the corresponding specimens (e–h) after thermal annealing at 150°C for 120 min, respectively. [Color figure can be viewed in the online issue, which is available at wileyonlinelibrary.com.]

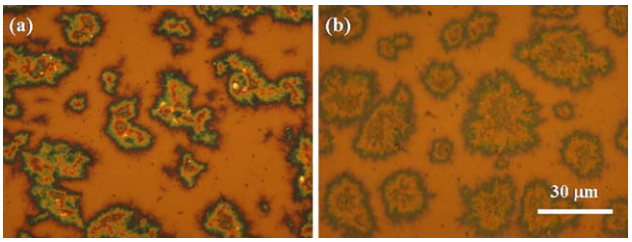


**Figure 8.** POM images of the films of (a) sPS/PCBM=1 : 1 and (b) sPS : P3HT : PCBM=1 : 1 : 1 after thermal annealing at 150°C for 120 min by soaking into cyclohexanone for 30 min to remove PCBM. [Color figure can be viewed in the online issue, which is available at wileyonlinelibrary.com.]

in Table I. It is observed that the CCL value of P3HT gradually decreases upon the incorporation of aPS.

### Morphology and Phase Structure of sPS/P3HT/PCBM Ternary Blending Films

Syndiotactic polystyrene shows of ordered phenyl rings packing in contrast to atactic polystyrene, and the interactions between sPS, P3HT, and PCBM should be different from those between aPS, P3HT, and PCBM. Moreover, the first and second heating curves for sPS and its blends show of significant change attributing to the different thermal history. In Figure 5(a), the sPS exhibit double exothermic peaks at 127.5°C and 272.7°C. After blending with P3HT, the melting peak ascribed to P3HT becomes less obvious, and the melting peak at 273.7°C corresponding to sPS could still be discerned. The P3HT and sPS are supposed to be immiscible, because of the crystallization of P3HT and sPS in separated regions. In the sPS/PCBM blend, the melting peaks of sPS and PCBM are less obvious as compared with the pristine specimens. The shift of sPS melting peak to about 263.8°C indicates the probable crystal-form transformation in the existence of PCBM molecules. Moreover, the melting peak of sPS at about 265.0°C could be still observed in the sPS/P3HT/PCBM ternary blend, illustrating that sPS is able to crystallize even in the presence of P3HT and PCBM.

Upon cooling from the melting state as shown in Figure 5(b), the sPS and P3HT crystallized separately in their blend, further revealing that the sPS and P3HT are immiscible. For the sPS/PCBM and sPS/P3HT/PCBM blends, only one crystallization peak at about 220.0°C could be discerned. The peak should be ascribed to sPS because of the fact that PCBM showed of no crystallization peak in aPS/PCBM blend. It is revealed that the crystallization of sPS was significantly restricted in the presence of PCBM. Figure 5(c) shows the second heating curves for sPS, P3HT, PCBM, and their blends. In the sPS/P3HT blend, both of P3HT and sPS exhibit the melting peaks. In the sPS/PCBM blend, the melting peak at around 263.8°C and 282.7°C is attributed to sPS and PCBM, respectively. In the sPS/P3HT/PCBM ternary blend, one major melting peak at 266.0°C corresponds to the melting of sPS. It is believed that the interactions between the components are strongly influenced by the tacticity of polystyrene.

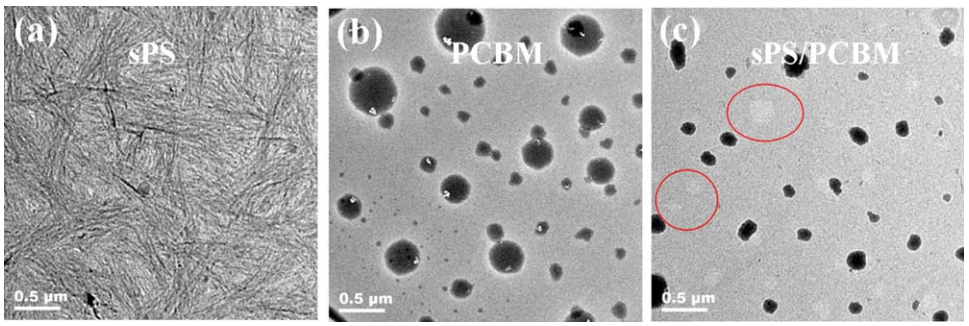


**Figure 9.** Transmission electron microscopy of (a) sPS, (b) PCBM and (c) sPS/PCBM (1 : 1) specimens. [Color figure can be viewed in the online issue, which is available at wileyonlinelibrary.com.]

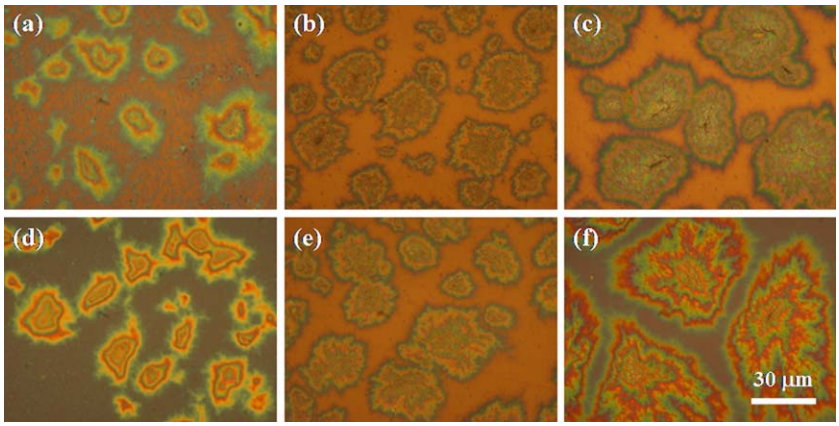


**Figure 10.** POM images of sPS/P3HT/PCBM ternary blending films, the as-cast specimens of (a–c) 1 : 3 : 3, 1 : 1 : 1, 3 : 1 : 1, and the specimens of (d–f) 1 : 3 : 3, 1 : 1 : 1, 3 : 1 : 1 after thermal annealing at 150°C for 120 min, respectively. [Color figure can be viewed in the online issue, which is available at wileyonlinelibrary.com.]

The crystalline structure of the ternary blend films was further characterized by GIXRD as shown in Figure 6. It is noted that the sPS exhibits two diffraction peaks at 14.2° and 17.0°, attributing to the α-form crystals.[41,42] Upon the incorporation of 3 wt % sPS, the diffraction peak of P3HT significantly increases, showing that a small amount of sPS facilitates the crystallization of P3HT. Further increase of sPS weight ratio eventually leads to the decrease of the intensity of P3HT diffraction peak, showing that the incorporation of high weight ratio of sPS may restrict the crystallization of P3HT. The crystallization behavior of P3HT in the sPS/P3HT/PCBM blend is inconsistent with that in aPS/P3HT/PCBM blend. Moreover, the position of the diffraction peak of P3HT shifts to lower angles, and the calculated lamellar spacing value increases from 1.63 to 1.75 nm. The diffraction peaks of sPS in the ternary blending films are difficult to be discerned, which is probably because of relatively low annealing temperature. Moreover, the CCL value of P3HT crystallites decreases upon incorporation of sPS.

To further investigate the morphology of the binary and ternary blends, the corresponding POM images are shown in Figure 7. For the pristine sPS, some crystalline aggregates distribute on the glass substrates. After blending with P3HT, the aggregates grow bigger and the visual field become less clear [Figure 7(b)]. It is speculated that the P3HT may migrate to the surface of the substrate with sPS on the bottom layer and P3HT phase on the upper layer. In sPS/PCBM blend [Figure 7(c)], the morphology of the aggregates is similar to that of pristine sPS, indicating the incorporation of PCBM molecules into the inner part of the aggregates. After thermal annealing at 150°C for 120 min, some anisotropic crystals grow out from the aggregates [Figure 7(g)]. After soaking into the cyclohexanone, the crystals disappear, revealing that the crystalline phase is because of the PCBM crystals. Moreover, some little light holes are left in the sPS aggregates, which illustrates that a part of PCBM molecules are wrapped up in the sPS aggregates (Figure 8). In the sPS/P3HT/PCBM ternary blend, the aggregates attributing to sPS dominate the whole image. No serious morphology change could be observed after thermal annealing treatment, illustrating that the PCBM molecules should be confined in the sPS phase and are

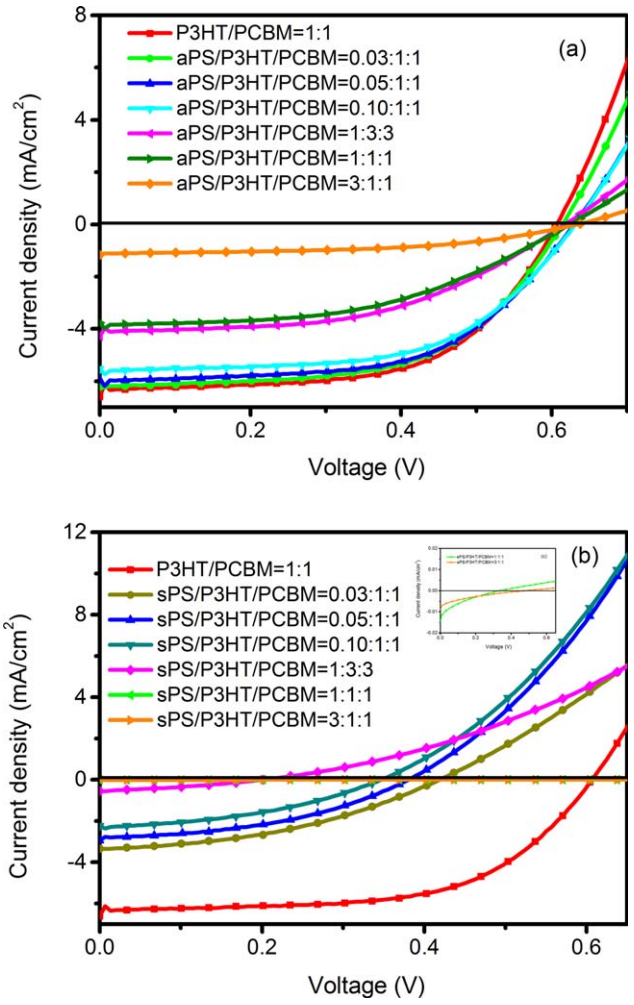


**Figure 11.** Photovoltaic curves of BHJ PSCs based on (a) aPS/P3HT/PCBM and (b) sPS/P3HT/PCBM blend films at different PS weight ratios after thermal annealing at 150°C for 10 min. (c) The enlarged figure of the *J–V* curve for sPS/P3HT/PCBM=1 : 1 : 1 and sPS/P3HT/PCBM=3 : 1 : 1 specimens. [Color figure can be viewed in the online issue, which is available at wileyonlinelibrary.com.]

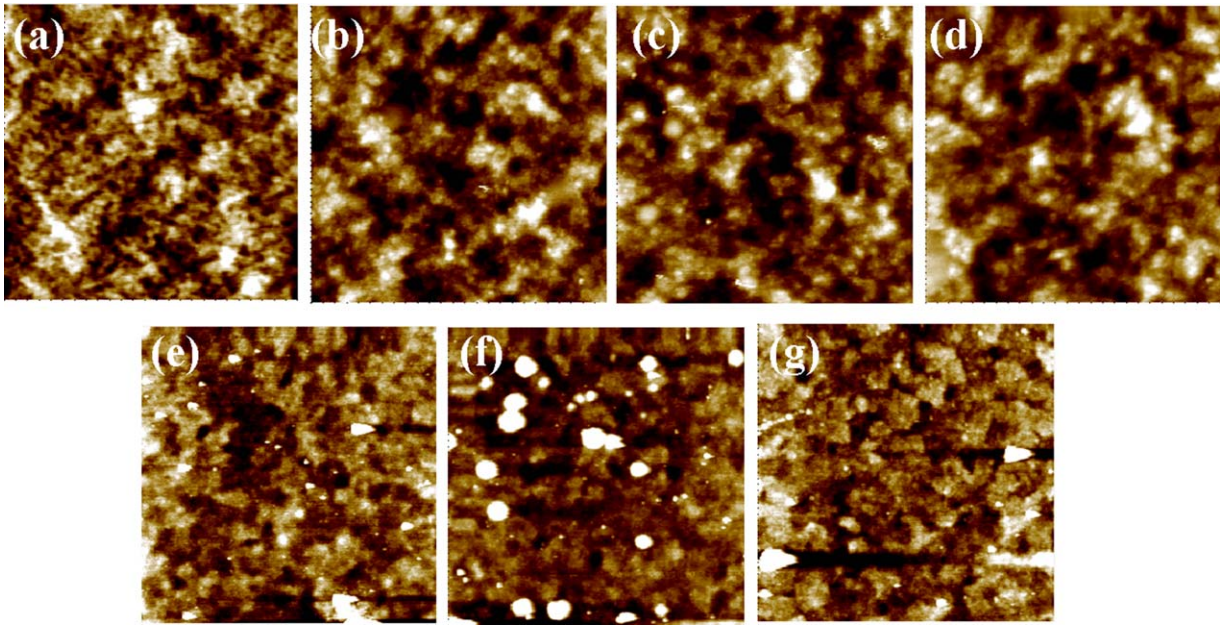


**Figure 12.** The AFM images of the (a) P3HT/PCBM, (b) aPS/P3HT/PCBM (0.03 : 1 : 1), (c) aPS/P3HT/PCBM (0.05 : 1 : 1), (d) aPS/P3HT/PCBM (0.10 : 1 : 1), (e) sPS/P3HT/PCBM (0.03 : 1 : 1), (f) aPS/P3HT/PCBM (0.05 : 1 : 1), and (g) aPS/P3HT/PCBM (0.10 : 1 : 1), respectively. The scan areas are 5×5 $\mu$m. [Color figure can be viewed in the online issue, which is available at wileyonlinelibrary.com.]

unable to crystallize because of the confinement of upper P3HT layer. It is believed that one additional P3HT layer should cover on the substrate or sPS surface. The TEM images shown in Figure 9 illustrate the morphology of sPS and its blend with PCBM. It is observed that the sPS form the fibrous structure while the PCBM molecules tend to aggregate to form spheres. By blending of sPS with PCBM, the PCBM clusters become irregular and smaller as compared with pristine PCBM. It is suggested that the morphology of PCBM aggregates could be modulated by sPS, and some of the PCBM clusters may be trapped in the inner part of sPS aggregates. The influence of sPS content on the morphology of ternary blend films is shown in Figure 10. By increase of the sPS weight ratio, the size of aggregates increases, and the color of the aggregates become deeper after thermal annealing.

**Photovoltaic Properties of Ternary Blends**

The performance of the solar cell based on PS/P3HT/PCBM system was measured, and the corresponding current/voltage ($J/V$) characteristics of the devices are illustrated in Figure 11, and Table I summarizes the PV parameters of the devices. The device fabricated using aPS/P3HT/PCBM at aPS weight ratio below 10 wt % exhibit PCE values similar to that of pristine P3HT/PCBM device of 2.3%. Additionally, the device based on aPS/P3HT/PCBM (1 : 3 : 3 and 1 : 1 : 1) blend exhibited a much lower PCE value of 1.3% and 1.2%, respectively. For the device based on aPS/P3HT/PCBM (3 : 1 : 1) blend, the PCE value of 0.4% could still be determined. The depression of the PCE value was mainly attributed to the decrease of $J_{sc}$ value because of the reduction of interfacial contact area between P3HT and electrode. Based on the POM observation, the migration of aPS onto the surface of the film may eventually restrict the electron transportation from the active layer to Al electrode. However, the slightly increasing of $V_{oc}$ may be attributed to soft insulating aPS lowering the leakage pathways as confirmed by the increase of shunt resistance. As far as the sPS/P3HT/PCBM system is concerned, the PCE value significantly decreased to 0.6% even at sPS weight ratio of 3 wt %. It is believed that the performance of the solar cell device is mainly determined by the morphology and phase structure of the active layer. Figure 12 shows the AFM images of aPS/P3HT/PCBM and sPS/P3HT/PCBM specimens. It is noted that surface morphology of films shows of no significant change upon incorporation of aPS. However, some of the bright dots contributing to highly crystalline phase are observed for the sPS/P3HT/PCBM specimens containing 5 and 10 wt % sPS. The phase-separated morphology for P3HT/PCBM specimen disappears upon the incorporation of sPS. It is suggested that the PCBM molecules might be trapped in the sPS phase, and the existence of sPS may play the role of impurities, restricting the exciton dissociation, as well as the charge transport in the P3HT/PCBM system.

The performance of the device should be also related with the absorption behavior of the active layer. Figure 13(a) displays the UV-vis absorption spectrum of P3HT/PCBM upon the incorporation of different amount of aPS. The spectrum of the P3HT/PCBM film shows a peak at 514 nm associated with the $\pi$–$\pi^*$ transition, two additional shoulders at 554 and 602 nm are contributed to the $\pi$–$\pi$ stacking of P3HT chains. By increasing of aPS weight ratio, the low energy absorption bands at 602 nm appears to increase in intensity, indicating that aPS could induce the crystallization of P3HT chains. Based on the POM images and soaking experiment, the aPS tended to migrate to the surface of films to form an insulating barrier layer and interrupt the transmission of the carrier, resulting in the significant reduce of $J_{sc}$ value for the aPS/P3HT/PCBM (3 : 1 : 1)

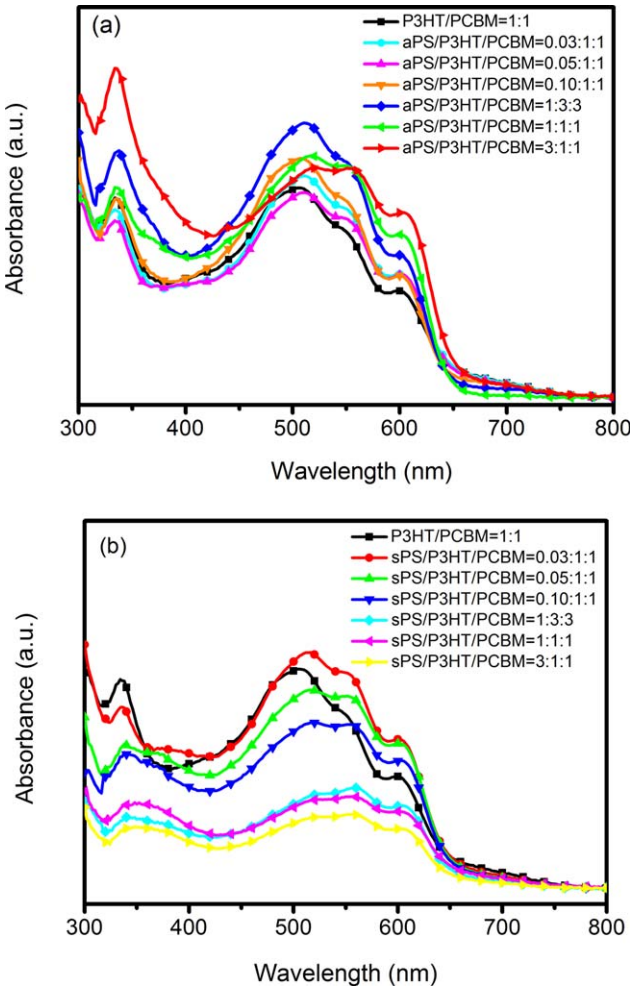


**Figure 13.** The UV-Vis absorption spectra of (a) aPS/P3HT/PCBM and (b) sPS/P3HT/PCBM blend films at different PS weight ratios after annealing at 150°C for 10 min. [Color figure can be viewed in the online issue, which is available at wileyonlinelibrary.com.]

specimen. The UV-vis absorption spectrum of sPS/P3HT/PCBM is shown in Figure 13(b). The relative intensity of the absorption peak at 602 nm reaches to the highest at sPS weight ratio of 3 wt %. Further increase of the sPS weight ratio eventually led to the decrease of the intensity of the absorption peak at 602 nm. The result indicates that a small amount of sPS facilitate the crystallization of P3HT while the large amount of sPS may impede the crystallization of P3HT, which is consistent with the GIXRD result.

## CONCLUSIONS

The interactions between polystyrene with different tacticities and P3HT and PCBM have been extensively investigated. The aPS was found to be immiscible with P3HT and restrict the crystallization of PCBM from the melting state. The aPS is found to induce the crystallization of P3HT at weight ratio below 50 wt % as revealed by GIXRD analysis. The lamellar spacing of P3HT increased from 1.63 to 1.76 nm and CCL value of P3HT gradually decreased upon incorporation of aPS. In the aPS/P3HT/PCBM ternary blend films, the morphology changed from nano-islands to spherical columnar domains to two-layer structure with increasing aPS content, and PCBM preferentially segregated to the interfaces between aPS and P3HT phase. The sPS is also immiscible with P3HT and able to crystallize in the presence of P3HT and PCBM. A small amount of sPS (3 wt %) facilitated the crystallization of P3HT while the incorporation of high weight ratio of sPS may eventually restrict the crystallization of P3HT. The PCE value of sPS/P3HT/PCBM significantly decreased to 0.6% even at sPS weight ratio of 3 wt %, attributing to the morphology change as observed by the AFM. The PCBM molecules could be incorporated in the sPS phase, and the sPS played the role of impurities, restricting the exciton dissociation, as well as the charge transport in the P3HT/PCBM system, resulting in a low PCE value.

## ACKNOWLEDGMENTS

Financial support for this work was provided by the National Natural Science Foundation of China (Grants 51303077), Ph.D. Programs Foundation for Young Teachers of Ministry of Education of China (Grants 20123601120010), Fund by State Key Laboratory of Luminescent Materials and Devices, South China University of Technology (Grants 2013-skllmd-04).

## REFERENCES

1. Morel, D. L.; Ghosh, A. K.; Feng, T.; Stogryn, E. L.; Purwin, P. E.; Shaw, R. F.; Fishman, C. *Appl. Phys. Lett.* **1978**, *32*, 495.
2. Tang, C. W. *Appl. Phys. Lett.* **1986**, *48*, 183.
3. Halls, J. J.; Walsh, M. C. A.; Greenham, N. C.; Marseglia, E. A.; Friend, R. H.; Moratti, S. C.; Holmes, A. B. *Nature* **1995**, *376*, 498.
4. Yu, G; Gao, J.; Hummelen, J. C.; Wudl, F.; Heeger, A. *J. Science* **1995**, *270*, 1789.
5. Bundgaard, E.; Krebs, F. C. *Sol. Energy. Mater. Sol. Cells* **2007**, *91*, 1019.
6. Tipnis, R.; Bernkopf, J.; Jia, S.; Krieg, J.; Li, S.; Storch, M.; Laird, D. *Sol. Energy Mater. Sol. Cells* **2009**, *93*, 442.
7. Verploegen, E.; Miller, C. E.; Schmidt, K.; Bao, Z.; Toney, M. F. *Chem. Mater.* **2012**, *24*, 3923.
8. Liao, H. C.; Tsao, C. S.; Lin, T. H.; Chuang, C. M.; Chen, C. Y.; Jeng, U.; Su, C. H.; Chen, Y. F.; Su, W. F. *J. Am. Chem. Soc.* **2011**, *133*, 13064.
9. Wu, W. R.; Jeng, U.; Su, C. J.; Wei, K. H.; Su, M. S.; Chiu, M. Y.; Chen, C. Y.; Su, W. B.; Su, C. H.; Su, A. C. *ACS Nano* **2011**, *5*, 6233.
10. Guan, X.; Zhang, K.; Huang, F.; Guillermo, C.; Cao, Y. *Adv. Funct. Mater.* **2012**, *22*, 2846.
11. Dang, M. T.; Hirsch, L.; Wantz, G. *Adv. Mater.* **2011**, *23*, 3597.
12. Li, G.; Yao, Y.; Yang, H.; Shrotriya, V.; Yang, G.; Yang, Y. *Adv. Funct. Mater.* **2007**, *17*, 1636.
13. Honda, S.; Nogami, T.; Ohkita, H.; Benten, H.; Ito, S. *ACS Appl. Mater. Interfaces* **2009**, *1*, 804.

14. Hori, T.; Masuda, T.; Fukuoka, N.; Hayashi, T.; Miyake, Y.; Kamikado, T.; Yoshida, H.; Fujii, A.; Shimizu, Y.; Ozaki, M. *Org. Electron.* **2012**, *13*, 335.
15. Wang, D. H.; Park, K. H.; Seo, J. H.; Seifter, J.; Jeon, J. H.; Kim, J. K.; Park, J. H.; Park, O. O.; Heeger, A. J. *Adv. Energy Mater.* **2011**, *1*, 766.
16. Paci, B.; Spyropoulos, G. D.; Generosi, A.; Bailo, D.; Albertini, V. R.; Stratakis, E.; Kymakis, E. *Adv. Funct. Mater.* **2011**, *21*, 3573.
17. Nismy, N. A.; Jayawardena, K. D. G. I.; Adikaari, A. A. D. T.; Silva, S. R. P. *Adv. Mater.* **2011**, *23*, 3796.
18. Stylianakis, M. M.; Mikroyannidis, J. A.; Kymakis, E. *Sol. Energy Mater. Sol. Cells.* **2010**, *94*, 267.
19. Goffri, S.; Müller, C.; Stingelin-Stutzmann, N.; Breiby, D. W.; Radano, C. P.; Andreasen, J. W.; Thompson, R.; Janssen, R. A. J.; Nielsen, M. M.; Smith, P.; Sirringhaus, H. *Nat. Mater.* **2006**, *5*, 950.
20. Müller, C.; Goffri, S.; Breiby, D. W.; Andreasen, J. W.; Chanzy, H. D.; Janssen, R. A. J.; Nielsen, M. M.; Radano, C. P.; Sirringhaus, H.; Smith, P.; Stingelin-Stutzmann, N. *Adv. Funct. Mater.* **2007**, *17*, 2674.
21. Wolfer, P.; Müller, C.; Smith, P.; Baklar, M. A.; Stingelin-Stutzmann, N. *Synth. Met.* **2007**, *157*, 827.
22. Sauvé, G.; McCullough, R. D. *Adv. Mater.* **2007**, *19*, 1822.
23. Madec, M. B.; Crouch, D.; Llorente, G. R.; Whittle, T. J.; Geoghegan, M.; Yeates, S. G. *J. Mater. Chem.* **2008**, *18*, 3230.
24. Qiu, L.; Lee, W. H.; Wang, X.; Kim, J. S.; Lim, J. A.; Kwak, D.; Lee, S.; Cho, K. *Adv. Mater.* **2009**, *21*, 1349.
25. Kumar, A.; Baklar, M. A.; Scott, K.; Kreouzis, T.; Stingelin-Stutzmann, N. *Adv. Mater.* **2009**, *21*, 4447.
26. Qiu, L.; Lim, J. A.; Wang, X.; Lee, W. H.; Hwang, M.; Cho, K. *Adv. Mater.* **2008**, *20*, 1141.
27. Kergoat, L.; Battaglini, N.; Miozzo, L.; Piro, B.; Pham, M. C.; Yassar, A.; Horowitz, G. *Org. Electron.* **2011**, *12*, 1253.
28. Wu, F. C.; Cheng, H. L.; Chen, Y. T.; Jang, M. F.; Chou, W. Y. *Soft. Matter.* **2011**, *7*, 11103.
29. Arias, A. C.; Endicott, F.; Street, R. A. *Adv. Mater.* **2006**, *18*, 2900.
30. Lee, J.; Jung, J. Y.; Kim, D. H.; Kim, J. Y.; Lee, B. L.; Park, J. I.; Chung, J. W.; Park, J. S.; Koo, B.; Jin, Y. W.; Lee, S. *Appl. Phys. Lett.* **2012**, *100*, 083302.
31. Ferenczi, T. A. M.; Müller, C.; Bradley, D. D. C.; Smith, P.; Nelson, J.; Stingelin, N. *Adv. Mater.* **2011**, *23*, 4093.
32. Wu, F. C.; Hsu, S. W.; Cheng, H. L.; Chou, W. Y.; Tang, F. C. *J. Phys. Chem. C.* **2013**, *117*, 8691.
33. Pan, C.; Li, H. F.; Bulent, A.; Satijia, S. K.; Zhu, Y. M.; Xu, D.; Ortiz, J.; Gersappe, D.; Rafailovich, M. H. *Macromolecules* **2013**, *46*, 1812.
34. Vohra, V.; Campoy-Quiles, M.; Garriga, M.; Murata, H. *J. Mater. Chem.* **2012**, *22*, 20017.
35. Xu, L.; Sharma, A.; Joo, S. W. *J. Phys. Chem. C* **2012**, *116*, 21615.
36. Ma, M.; He, Z. K.; Yang, J. H.; Wang, Q.; Chen, F.; Wang, K.; Zhang, Q.; Deng, H.; Fu, Q. *Langmuir* **2011**, *27*, 1056.
37. Rastogi, S.; Goossens, J. G. P.; Lemstra, P. *J. Macromolecules* **1998**, *31*, 2983.
38. Moulton, J.; Smith, P. *J. Polym. Sci. Part B: Polym. Phys.* **1992**, *30*, 871.
39. Nicho, M. E.; García-Escobar, C. H.; Arenas, M. C.; Altuzar-Coello, P.; Cruz-Silva, R.; Güizado-Rodríguez, M. *Mater. Sci. Eng. B* **2011**, *176*, 1393.
40. Roe, R. J. Ed. Methods of X-Ray and Neutron Scattering in Polymer Science; Oxford University Press: UK, **2000**.
41. Itagaki, H.; Mochizuki, J. *Macromolecules* **2005**, *38*, 9625.
42. Zhou, W. H.; Lu, M.; Mai, K. C. *Polymer* **2007**, *48*, 3858.